# Electrohydrodynamic instability of a capacitive elastic membrane

Y.-N. Young and Michael J. Miksis

Citation: Physics of Fluids (1994-present) **27**, 022102 (2015); doi: 10.1063/1.4907936
View online: http://dx.doi.org/10.1063/1.4907936
View Table of Contents: http://scitation.aip.org/content/aip/journal/pof2/27/2?ver=pdfcov
Published by the AIP Publishing

PHYSICS OF FLUIDS **27**, 022102 (2015)

# Electrohydrodynamic instability of a capacitive elastic membrane

Y.-N. Young[1,a] and Michael J. Miksis[2]
[1]*Department of Mathematical Sciences and Center for Applied Mathematics and Statistics, New Jersey Institute of Technology, Newark, New Jersey 07102, USA*
[2]*Department of Engineering Sciences and Applied Mathematics, Northwestern University, Evanston, Illinois 60208, USA*

(Received 6 September 2014; accepted 27 January 2015; published online 13 February 2015)

The electrohydrodynamic instability of a leaky (weakly conducting) capacitive elastic membrane driven by a direct current electric field, both perpendicular and parallel to the membrane in a micro-fluidic channel, is investigated theoretically. In the leaky dielectric framework, electric charges can accumulate on either side of the membrane, and the effect of the accumulated surface charge depends on the ratio of charge relaxation time in the bulk to the membrane charging time. Under a parallel electric field, a non-conducting membrane can become unstable while under a perpendicular electric field a non-conducting capacitive membrane is always stable and membrane conductance is essential for the membrane instability. The effects of membrane conductance, bending modulus, and charge relaxation time on the membrane instability are elucidated for several combinations of conductivity ratio and permittivity ratio in the bulk fluids. Regions of instability are computed for both the parallel and perpendicular electric fields. The tangential electric field acts similarly to the membrane tension in terms of its damping effects at small length scales (high wave number), while either bending or membrane tension is needed to damp out the small-scale perturbations under a perpendicular electric field. © *2015 AIP Publishing LLC.* [http://dx.doi.org/10.1063/1.4907936]

## I. INTRODUCTION

Electric fields have been extensively utilized to drive a fluid interface or a lipid bilayer membrane unstable for fabrication of micron-sized droplets[1–4] or vesicles in microfluidic channels.[5–8] For the micro-droplet formation from a fluid interface between two layers, a channel flow is often employed to collect droplets from the electrohydrodynamic instability of the fluid interface driven by an external electric field. In these micro-fluidic systems, the Reynolds number is very small and hence the Stokesian regime is appropriate to describe the fluid motion. At zero Reynolds number, the interface between two fluids under a channel Poiseuille flow is always stable when each layer is of equal depth,[9] therefore the observed electrohydrodynamic instability in Ref. 1 is most likely due to the mismatch in electric properties and the resultant fluid interface instability under an electric field. Linear stability on a fluid interface subject to an external electric field gives a good estimate for the size of the droplet that ensues from the interface instability.[10–13] Regions of instability have been identified in terms of ratios of electric permittivity and conductivity between the two layers. In particular, these unstable regions are divided into sub-regions where the normal or parallel electric field is dominant and gives the larger growth rate.[12,13]

A lipid bilayer membrane consists of two layers of lipid molecules, with their hydrophilic heads interacting with solvent molecules in the bulk (see Figure 1). The membrane thickness is approximately 5 nm, and the lipid-lipid interaction gives rise to membrane elasticity and tension. In

[a]yyoung@njit.edu

 

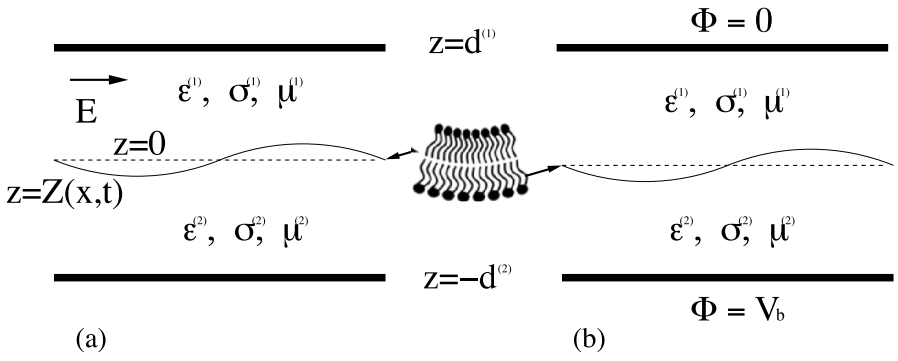


FIG. 1. A planar lipid bilayer membrane (at height $z = Z(x, t)$) separates two layers of leaky dielectric fluid. The bulk fluid is characterized by permittivity ($\varepsilon$), conductivity ($\sigma$), and viscosity ($\mu$). (a) The imposed electric field **E** is tangential to the unperturbed, flat membrane. (b) The electric potential $\Phi$ is fixed on the top electrode ($\Phi = 0$) and bottom electrode ($\Phi = V_b$).

the continuum modeling framework, a lipid bilayer membrane is often modeled as an elastic sheet with a tension that relates to the incompressibility of the membrane area.[14] The Helfrich membrane energy $\mathcal{F} = \int_\Omega \left(\frac{\kappa_b}{2} H^2 + \gamma\right) d\Omega$ (where $\Omega$ is the membrane surface, $\gamma$ is the membrane tension, $\kappa_b$ is the bending modulus, and $H$ is the mean curvature) is often adopted for the computation of membrane forces. Under an electric field, the membrane behaves like a leaky capacitor as it is impermeable to ions unless there are pores or ion channels across the membrane. Depending on the degree of membrane poration or membrane constituents (such as transmembrane ion channels), there may be transmembrane currents due to a finite membrane conductance (leakage). Consequently, the transmembrane potential varies over the "membrane capacitor charging" time under an electric field, unlike the fluid interface where the electric potential is continuous (corresponding to an infinite conductance).

For vesicle formation from a planar membrane subject to an external electric field (also referred to as electroformation of vesicles), the relevant chemical processes (prior to the membrane instability) further complicate the physical processes of vesicle formation. For example, often multiple planar membranes interact with each other before individual lipid membranes interact with solvents and deform due to the external electric field. Recently, Young *et al*. conducted a long-wave analysis on a planar lipid bilayer membrane under an electric field normal to the membrane.[15] Prior to instability, the tension of the flat membrane is assumed to be negligible, and the condition for electrohydrodynamic instability of a capacitive elastic membrane under a direct current (DC) electric field is found to be similar to that for a fluid interface. In addition, the effect of an alternating current (AC) normal electric field is also investigated. At low AC frequencies, the membrane can be unstable even with zero membrane conductance. As the AC field magnitude is increased, the nonlinear dynamics ensued from the electrohydrodynamic instability is found to exhibit three types of motion: membrane undulation, membrane flip-flop, and a traveling wave on the membrane.[15]

There has been prior work investigating effects of a normal electric field on the electrohydrodynamic instability of a non-conducting planar membrane[16] and a conducting planar membrane.[17] Under a normal electric field, the non-conducting membrane is always stable while the conducting membrane can be unstable for parameters in certain regions. To our knowledge, the effect of an electric field tangent to the membrane has not been theoretically investigated. In this work, we focus on the tangential (parallel) electric field case but we also present results for the normal (perpendicular) electric field case for comparison. Before the external electric field is turned on, a flat membrane is freely suspended in leaky dielectric fluids, and therefore the membrane tension is very small prior to the instability. In the formulation here we keep the membrane tension, this will allow us to investigate limits where we recover a fluid interface. Although the tension is close to zero for a planar membrane it can be nonzero for a deformed membrane, and hence keeping it in the formulation allows for a more general statement of the model. We will then focus on regions of instability for a planar membrane under an electric field. The paper is organized as follows. Section II presents the mathematical model for the electrohydrodynamic instability of a capacitive

lipid bilayer under an electric field in a channel. Section III presents the linear stability results, and conclusions are drawn in Sec. IV.

## II. FORMULATION OF THE PHYSICAL AND MATHEMATICAL MODEL

The stability of a planar capacitive membrane immersed between two immiscible, viscous, incompressible leaky dielectric fluids subject to an external electric field is investigated. A schematic of the model is shown in Figure 1, where $\mu$ is the fluid viscosity, $\sigma$ is the electrical conductivity, and $\varepsilon^{(j)}$ is the electrical permittivity of the fluid. The geometry for the tangential electric field case is illustrated in Figure 1(a), while the normal electric field case is illustrated in Figure 1(b). Note that the superscript 1(2) is associated with variables related to the top (bottom) layer, respectively, in Figure 1, while the subscript "$m$" in the following refers to membrane variables. Without loss of generality, we will focus mostly on $\sigma_r \equiv \sigma^{(1)}/\sigma^{(2)} \leq 1$ for the parallel case.

The typical thickness of a lipid bilayer membrane is $d_m \approx 5$ nm. This thinness allows us to model the interface on the macroscopic scale as an infinitesimally thin membrane (see Figure 1) with a bending modulus $\kappa_b \approx 21 k_B T$. For a lipid-bilayer membrane, lipid-lipid interactions are so strong that the membrane is usually assumed to be incompressible, i.e., there is local conservation of surface area.[14] With this assumption, the tension needs to be a variable chosen to force this constraint.[14] We will consider this incompressible membrane (IM) case here but we will also consider the case where the tension is a constant and the surface incompressibility condition is not enforced. There have been several investigations using both of these models[18] and here we would like to give a better understanding of the differences between them. We will refer to a membrane where the surface incompressibility is not enforced as simply an elastic sheet (ES).

Ions are mostly impermeable to the lipid bilayer membrane except through trans-membrane ion channels or pores. Therefore, a bilayer membrane acts as a capacitor under an electric field with a capacitance $C_m = \varepsilon_m/d_m \approx 0.01$ F/m$^2$ and a conductance $G_m = \sigma_m/d_m \approx 10^{-3} - 10^6$ S/m$^2$, depending on the degree of electric leakage. As $d_m$ is much smaller than the characteristic length of the system, the lipid bilayer membrane is often modeled as a capacitive elastic sheet with an effective capacitance $C_m$ and the membrane conductance $G_m$.

There are several time scales involved in this system. In the leaky dielectric framework, the bulk charge relaxes over a time $t_c^{(j)} = \varepsilon^{(j)}/\sigma^{(j)} \sim 1$ $\mu$s for aqueous systems. This time scale is much smaller than any other time scale in this system, and therefore the bulk charge is effectively zero in the leaky dielectric framework. The capacitive membrane charges on a time scale[19] $t_m = \frac{C_m d}{\sigma^{(2)}} \frac{1+\sigma_r}{1+g_m(1+\sigma_r)} \sim 1$ ms with $g_m = G_m d/\sigma^{(2)}$, and $d$ a characteristic channel height. The balance between viscous stress and the electric shear traction gives the time scale $t_{EHD}^{(j)} = \frac{\mu^{(j)}}{\varepsilon^{(j)} E_0^2}$ with $E_0$ a characteristic magnitude of the applied electric field. The bending resistance to changes in membrane curvature gives another time scale $t_\kappa^{(j)} = \frac{\mu^{(j)}}{\kappa_b Q^3}$ for a membrane undulation wave number $Q$. Typical values for the physical parameters yield $t_\kappa \gg t_{EHD}$ and $t_m \approx t_{EHD}$, but phenomena on these time scales are retained in the model. With these parameter values, the model developed in Refs. 15–17 for a capacitive elastic membrane is justified and will be used here.

### A. Model for a capacitive elastic membrane in leaky dielectric framework

The model is formulated following Refs. 15, 17, and 19. The electric field is given by $\mathbf{E}^{(j)} = -\nabla\Phi^{(j)}$, where $\Phi$ is the electric potential. Within the leaky dielectric framework, the bulk charge density is zero in the fluids, therefore $\Phi$ satisfies in the fluids the Laplace equation

$$\nabla^2\Phi^{(j)} = 0 \quad j = 1,2. \tag{1}$$

Within each fluid, the two-dimensional fluid velocity $\mathbf{v}^{(j)} = (u^{(j)}, w^{(j)})$ satisfies the incompressible Stokes equations

$$-\nabla p^{(j)} + \mu^{(j)}\nabla^2\mathbf{v}^{(j)} = 0, \tag{2}$$

$$\nabla \cdot \mathbf{v}^{(j)} = 0, \tag{3}$$

where $p^{(j)}$ is pressure. On the channel walls $\mathbf{v}^{(1)}(z = d^{(1)}) = 0$ and $\mathbf{v}^{(2)}(z = -d^{(2)}) = 0$. Let $z = Z(x,t)$ denote the membrane. At the membrane, the tangential velocity is continuous: $[\mathbf{v}^{(j)} \cdot \hat{t}]_2^1 = 0$ with $[f]_2^1 \equiv f^{(1)} - f^{(2)}$ denoting the jump in the variable $f$ across the membrane. The kinematic condition at the membrane gives $[\mathbf{v}^{(j)} - \mathbf{U}] \cdot \hat{n} = 0$ with $\mathbf{U}$ the membrane velocity. The normal and tangential stress balances at the membrane are

$$\left[p^{(j)} - \hat{n}\left(\mathbf{e}^{(j)} + \varepsilon^{(j)}\left(\mathbf{E}^{(j)}\mathbf{E}^{(j)} - \frac{1}{2}|\mathbf{E}^{(j)}|^2\mathbf{I}\right)\right)\hat{n}\right]_2^1 = 2\gamma H - 2\kappa_b\nabla_s^2 H - 4\kappa_b H^3, \tag{4}$$

$$\left[\hat{n}\left(\mathbf{e}^{(j)} + \varepsilon^{(j)}\mathbf{E}^{(j)}\mathbf{E}^{(j)}\right)\hat{t}\right]_2^1 = \nabla_s\gamma, \tag{5}$$

where $\mathbf{e}^{(j)} \equiv \mu^{(j)}(\nabla\mathbf{v}^{(j)} + (\nabla\mathbf{v}^{(j)})^T)$ is the viscous stress tensor, $\gamma$ is the membrane tension, $\kappa_b$ is the membrane bending modulus, and $H = Z_{xx}/2(1 + Z_x^2)^{1.5}$ is the curvature of the planar membrane. For the lipid bilayer membrane, the tension $\gamma$ arises from interactions between lipids as the membrane deforms under stress. The conservation of total number of lipids in the membrane implies that the local membrane area remains (close to) constant as the membrane is under stress and/or deforms,[14] i.e., the surface is incompressible. Therefore, the membrane tension may be spatially non-homogeneous, and hence the Marangoni stress term on the right hand side of Eq. (5). The tension is now determined by forcing the additional incompressibility constraint along the interface

$$\nabla_s \cdot \mathbf{U} = 0, \tag{6}$$

where $\nabla_s$ is the surface divergence operator and $\mathbf{U}$ is the velocity along the interface. In the case of an elastic sheet, the interface is not incompressible and the tension is a known constant, hence there is no need for the additional Eq. (6).

Under the imposed electric field, the current across the bilayer membrane can be considered as follows. First, we consider the conservation of normal current density across the membrane facing the top fluid (superscript "1") and then facing the bottom fluid (superscript "2"), respectively. Here, we distinguish between each of the monolayers along the bilayer for the sake of this derivation but within our continuum model the bilayer lipid membrane interface has zero thickness and is located at $z = 0$ before any perturbation. This results in the two conservation equations along the membrane

$$\mathbf{n} \cdot (\mathbf{J}^{(1)} - \mathbf{J}_m) = -\frac{\partial q^{(1)}}{\partial t} - \nabla_s \cdot (\mathbf{U}q^{(1)}) \quad \text{facing fluid "1,"} \tag{7}$$

$$\mathbf{n} \cdot (\mathbf{J}_m - \mathbf{J}^{(2)}) = -\frac{\partial q^{(2)}}{\partial t} - \nabla_s \cdot (\mathbf{U}q^{(2)}) \quad \text{facing fluid "2."} \tag{8}$$

Here, $\mathbf{J}^{(i)} = \sigma^{(i)}\mathbf{E}^{(i)}$ represents current density, $q^{(i)}$ denotes the electric charge density along each side, $\mathbf{J}_m = \sigma_m\mathbf{E}_m$ is the ohmic current density crossing the membrane, and $\mathbf{E}_m$ is the electric field within the membrane. The current leaking through the membrane $\mathbf{n} \cdot \mathbf{J}_m$ will be approximated by the voltage jump across the membrane times the membrane conductivity, i.e., $\mathbf{n} \cdot \mathbf{J}_m = G_m V_m$, where $V_m = \Phi^{(2)} - \Phi^{(1)}$ is the transmembrane potential. The right hand side of both (7) and (8) represents the rate of change of charge along the monolayer of the moving interface. The surface charge density along the top of the membrane is given by $q^{(1)} = \varepsilon^{(1)}\mathbf{n} \cdot \mathbf{E}^{(1)} - \varepsilon_m\mathbf{n} \cdot \mathbf{E}_m = \varepsilon^{(1)}\mathbf{n} \cdot \mathbf{E}^{(1)} - C_m V_m$ at $z = Z^+$, where the approximation $\varepsilon_m\mathbf{n} \cdot \mathbf{E}_m = C_m V_m$ is used for a thin capacitive membrane. Similarly, along the bottom side of the membrane at $z = Z^-$ we have $q^{(2)} = C_m V_m - \varepsilon^{(2)}\mathbf{n} \cdot \mathbf{E}^{(2)}$. Note that this implies that the total charge is $q = q^{(1)} + q^{(2)} = \varepsilon^{(1)}\mathbf{n} \cdot \mathbf{E}^{(1)} - \varepsilon^{(2)}\mathbf{n} \cdot \mathbf{E}^{(2)}$. Rearranging Eqs. (7) and (8), we obtain the governing equation for the transmembrane potential $V_m$ along $z = Z$ as

$$C_m\frac{dV_m}{dt} + G_m V_m = \sigma^{(1)}\mathbf{n} \cdot \mathbf{E}^{(1)} + \varepsilon^{(1)}\frac{d\left(\mathbf{n} \cdot \mathbf{E}^{(1)}\right)}{dt} = \sigma^{(2)}\mathbf{n} \cdot \mathbf{E}^{(2)} + \varepsilon^{(2)}\frac{d\left(\mathbf{n} \cdot \mathbf{E}^{(2)}\right)}{dt}, \tag{9}$$

where $\frac{d}{dt}$ denotes the material derivative. For the electric potential, two boundary conditions at the membrane are given in Eq. (9). Two other boundary conditions for the electric potential $\Phi$ are on the channel walls: $\frac{\partial\Phi^{(j)}}{\partial z} = 0$ on the walls for an external electric field parallel to the flat membrane;

while $\Phi^{(1)} = 0$ at $z = d^{(1)}$, and $\Phi^{(2)} = V_b$ at $z = -d^{(2)}$ for an external electric field normal to the flat membrane.

The physical parameters with superscripts are defined in Figure 1 and the caption. The governing equations are rendered dimensionless by the following scalings: $d^{(2)}$, $d^{(2)}/U_0$, $U_0$ $(=\sigma^{(2)}/C_m)$, $V_b$, $\mu^{(2)}U_0/d^{(2)}$, and $V_b/d^{(2)}$ for length, time, velocity, voltage, pressure, and charge density, respectively. The applied electric voltage is $V_b \equiv E_0 d^{(2)}$. The resultant dimensionless parameters are $d_r = d^{(1)}/d^{(2)}$, $\varepsilon_r = \varepsilon^{(1)}/\varepsilon^{(2)}$, $\sigma_r = \sigma^{(1)}/\sigma^{(2)}$, $\mu_r = \mu^{(1)}/\mu^{(2)}$, $Ca = \mu^{(2)}U_0/\gamma_0$, $E_b = \varepsilon^{(2)}V_b^2/(\mu^{(2)}U_0 d^{(2)})$, $\kappa = \kappa_b C_m/(\mu^{(2)}\sigma^{(2)}d^{(2)2})$, $S = d^{(2)}\sigma^{(2)}/(U_0\varepsilon^{(2)}) = \frac{\varepsilon_m}{\varepsilon^{(2)}}\frac{d^{(2)}}{d_m}$, and $g_m = G_m d^{(2)}/\sigma^{(2)}$. Typical physical parameter values for a lipid bilayer membrane are for the conductivity $\sigma_m \approx 10^{-9} - 10^{-3}$ S m$^{-1}$, $\varepsilon_m \approx 5 \times 10^{-11}$ F m$^{-1}$, $\kappa_b \approx 10^{-19}$ J, $d^{(2)} \approx 10^{-3} - 1$ mm, $\sigma \approx 10^{-6} - 10^{-3}$ S m$^{-1}$, and $\mu \approx 0.1 - 1$ Pa s. The membrane tension for an unstressed planar membrane is as low as $10^{-9}$ N m$^{-1}$. These units imply that the dimensionless bending rigidity can vary as $10^{-12} \le \kappa \le 10^{-6}$, while the Capillary number can vary as $10^4 \le Ca \le 10^7$. The Capillary number for an ES is also very large as the tension of a flat elastic sheet is small.[20] However, the Capillary number is kept in the following formulation to help elucidate the various effects on the electrohydrodynamic instability of an IM (or ES) under an electric field.

Our aim is to investigate the linear stability of a membrane governed by Eqs. (1)–(9). Both the IM and ES cases will be considered. Prior to the perturbation, the base state is a flat membrane acted on by a uniform tangential electric field $\mathbf{E} = E_0\mathbf{x}$, or a steady normal electric field defined by the potentials along the two parallel electrodes at $z = d^{(1)}$ and $z = -d^{(2)}$ plus the capacitive boundary conditions (9) along the flat membrane.

### B. The base state and the linearized equations

For a capacitive membrane under an electric field parallel to the membrane (Figure 1(a)), the base state for the flat membrane, $z = Z_0 = 0$, is given by

$$\mathbf{v}_0^{(j)} = 0, \quad \frac{\partial \Phi_0^{(j)}}{\partial x} = -1, \quad q_0 = 0, \text{ and } V_{m0} = 0, \tag{10}$$

where the superscript $j = 1$ (2) is for the upper (lower) fluid, and subscript "0" denotes the base state. For the case where the electric field is normal to the flat membrane, the base state is

$$\Phi_0^{(1)} = \frac{g_m}{g_m(d_r + \sigma_r) + \sigma_r}(-z + d_r), \quad \Phi_0^{(2)} = \frac{1}{g_m(d_r + \sigma_r) + \sigma_r}\left(-g_m\sigma_r z + d_r g_m + \sigma_r\right), \tag{11}$$

$$q_0 = \frac{g_m\left(\varepsilon_r - \sigma_r\right)}{g_m(d_r + \sigma_r) + \sigma_r}, \text{ and } V_{m0} = \frac{\sigma_r}{g_m(d_r + \sigma_r) + \sigma_r}, \tag{12}$$

for $-1 \le z \le d_r$.

Perturbations to the base state are assumed periodic in $x$ in the form $f_1(z)e^{ikx+\omega t} + c.c.$ with $k$ the dimensionless wave number and $\omega$ the dimensionless growth rate of the perturbation. Note that variables with a subscript 1 are the amplitudes of the perturbation to the basic state. After substituting these perturbations into the evolution Eqs. (1)–(3), the governing linearized equations are

$$-ikp_1^{(j)} + \mu_r\left(\frac{d^2u_1^{(j)}}{dz^2} - k^2u_1^{(j)}\right) = 0, \tag{13}$$

$$-\frac{dp_1^{(j)}}{dz} + \mu_r\left(\frac{d^2w_1^{(j)}}{dz^2} - k^2w_1^{(j)}\right) = 0, \tag{14}$$

$$iku_1^{(j)} + \frac{dw_1^{(j)}}{dz} = 0, \tag{15}$$

$$\frac{d^2\Phi_1^{(j)}}{dz^2} - k^2\Phi_1^{(j)} = 0. \tag{16}$$

Equations (13), (14), and (15) can be combined into a fourth order equation for $w_1^{(j)}$, and the solutions $w_1^{(j)}$ and $\Phi^{(j)}$ can be expressed as

$$w_1^{(j)} = A^{(j)}e^{kz} + B^{(j)}e^{-kz} + a^{(j)}ze^{kz} + b^{(j)}ze^{-kz}, \tag{17}$$

$$\Phi_1^{(j)} = C^{(j)}\cosh(kz) + D^{(j)}\sinh(kz). \tag{18}$$

The twelve coefficients ($j = 1,2$), along with the growth rate $\omega$, are determined from the boundary conditions.

For an elastic incompressible membrane, the surface-incompressibility (Eq. (6)) dictates that (at the linear order) the tangential component of the velocity vanishes on either side of the membrane, i.e., $u^{(j)} = 0$ along $z = 0$. Thus, the boundary conditions for the perturbed velocity follow from the equations in Sec. II A and are given by

$$u_1^{(j)} = 0 = w_1^{(j)} \text{ on the channel walls,} \tag{19a}$$

$$w_1^{(j)} = \omega Z_1 \text{ on } z = 0, \tag{19b}$$

where $Z_1 e^{ikx+\omega t}$ is the perturbed membrane profile. Along $z = 0$, the membrane incompressibility condition Eq. (6) for the IM case gives at linear order

$$u^{(1)} = u^{(2)} = 0, \tag{20}$$

while the continuity of the tangential velocity for the ES case gives

$$\left[u^{(j)}\right]_2^1 = 0. \tag{21}$$

Other boundary conditions depend on the direction of the external electric field. For a parallel electric field, they are

$$\frac{d\Phi_1^{(j)}}{dz} = 0 \text{ on channel walls,} \tag{22}$$

$$\left[\sigma_r^{(j)}\left(ikZ_1 + \frac{d\Phi_1^{(j)}}{dz}\right)\right]_2^1 = \frac{1}{S}\omega q_1, \tag{23}$$

$$(\omega + g_m)V_{m1} = \left(1 + \frac{\omega}{S}\right)\mathbf{n}\cdot\mathbf{E}_1^{(2)}, \tag{24}$$

$$\left[\mu_r^{(j)}\left(\frac{du_1^{(j)}}{dz} + iku_1^{(j)}\right) + \varepsilon_r^{(j)}E_b\left(\frac{d\Phi_1^{(j)}}{dz} + ikZ_1\right)\right]_2^1 = ik\gamma_1, \tag{25}$$

$$\left[p_1^{(j)} - 2\mu_r^{(j)}\frac{dw_1^{(j)}}{dz} + \varepsilon_r^{(j)}E_b ik\Phi_1^{(j)}\right]_2^1 = -\frac{k^2}{Ca}Z_1 - \kappa k^4 Z_1, \tag{26}$$

where $\mu_r^{(1)} \equiv \mu_r$, $\sigma_r^{(1)} \equiv \sigma_r$, $\varepsilon_r^{(1)} \equiv \varepsilon_r$, $\mu_r^{(2)} = 1$, $\sigma_r^{(2)} = 1$, $\varepsilon_r^{(2)} = 1$, $\mathbf{n}\cdot\mathbf{E}_1^{(2)} = -ikZ_1 - \frac{d\Phi_1^{(2)}}{dz}$, and

$$q_1 = \left[\varepsilon_r^{(j)}\left(-ikZ_1 - \frac{d\Phi_1^{(j)}}{dz}\right)\right]_2^1. \tag{27}$$

For a normal electric field, the boundary conditions become

$$\Phi_1^{(j)} = 0 \text{ on channel walls,} \tag{28}$$

$$\left[\sigma_r^{(j)}\left(\frac{d\Phi_1^{(j)}}{dz}\right)\right]_2^1 = \frac{1}{S}\left(\omega q_1 + iku_1^{(2)}q_0\right), \tag{29}$$

$$(\omega + g_m)V_{m1} = \left(1 + \frac{\omega}{S}\right)\mathbf{n}\cdot\mathbf{E}_1^{(2)}, \tag{30}$$

$$\left[\mu_r^{(j)}\left(\frac{du_1^{(j)}}{dz}+ikw_1^{(j)}\right)+\varepsilon_r^{(j)}E_b\frac{\partial\Phi_0^{(j)}}{\partial z}\left(ik\Phi_1^{(j)}+ik\frac{\partial\Phi_0^{(j)}}{\partial z}Z_1\right)\right]_2^1=ik\gamma_1, \tag{31}$$

$$\left[p_1^{(j)}-2\mu_r^{(j)}\frac{dw_1^{(j)}}{dz}-\varepsilon_r^{(j)}E_b\frac{d\Phi_0^{(j)}}{dz}\frac{\Phi_1^{(j)}}{dz}\right]_2^1=-\frac{k^2}{Ca}Z_1-\kappa k^4Z_1, \tag{32}$$

where $\mathbf{n}\cdot\mathbf{E}_1^{(2)}=-\frac{d\Phi_1^{(2)}}{dz}|_{z=0}$,

$$q_1=\left[\varepsilon_r^{(j)}\left(-\frac{d\Phi_1^{(j)}}{dz}\right)\right]_2^1, \tag{33}$$

and $V_{m1}=\Phi_0^{(2)}-\Phi_0^{(1)}+Z_1\left(\frac{d\Phi_0^{(2)}}{dz}-\frac{\Phi_0^{(1)}}{dz}\right)$. Equations (22) and (28) are the boundary conditions for the electric potential (one for each layer) on the channel walls, and all the other boundary conditions are evaluated along the unperturbed flat interface.

The linearized system consists of Eqs. (13)–(21) and (22)–(26) for the parallel electric field case. For the normal electric field case, the governing linear equations are Eqs. (13)–(21) and (28)–(32). It is straightforward to solve each of these systems of equations for the growth rate $\omega$. The result will be a cubic equation for $\omega$ which depends on wave number $k$ and all the physical parameters. For the special case of $1/S=0$, i.e., the charge convection along the interface is negligible, the equation becomes a quadratic equation in $\omega$ (see, e.g., Ref. 17 for the normal electric field case). In the Appendix, we present this quadratic equation explicitly for the case of an incompressible membrane subject to a parallel electric field with negligible charge convection ($1/S=0$) and $d_r=1$. Computational results are presented for all other cases. These computations were done by first using Mathematica to identify the growth rate as a function of all physical parameters and wave number, and then using MatLab to plot the dispersion curve.

It should be noted that in the IM case, the tension perturbation $\gamma_1$ only appears in Eq. (25) for the parallel field case and in Eq. (31) for the normal electric field case. This means that in the IM case, the linear stability is independent of these tangential stress conditions and we do not have to consider these equations further in our analysis. The reason for this is that the zero tangential velocity constraint on the membrane has introduced an additional condition allowing us to determine the stability. Note that in the ES case, we only have that the continuity in the tangential velocity: one less condition than the incompressible case. Hence the tension must be considered a known, in particular a constant, and the tangential stress conditions (25) and (31) are needed to determine stability in general.

It is interesting to note that the parameter $S$ is very large in general and several investigations[10,12,13,15,17,19] have used this to simplify the capacitive system by setting to zero the right hand side of (23) and (29). The dimensionless parameter $S$ is the ratio of the membrane charging time to the bulk charge relaxation time $S=t_m/t_c^{(2)}$, which is the product of the two ratios $\frac{\varepsilon_m}{\varepsilon^{(2)}}\frac{d^{(2)}}{d_m}$. For a lipid bilayer membrane $d^{(2)}/d_m\sim O(10^3)$, $\varepsilon_m/\varepsilon^{(2)}\sim 0.01$–$0.1$, hence $S\sim 10-100$ for a micro-fluidic channel filled with leaky dielectric fluids separated by a planar lipid bilayer membrane. In Secs. III B and III C, we will demonstrate that the limit $S\gg 1$ is asymptotically reached as long as $S$ is of the order of several hundreds.

As noted earlier, the tension of a flat membrane freely suspended in a fluid is often very small prior to significant membrane deformations. Hence, the terms containing the capillary number could be neglected in this linear analysis but we will retain it here, and unless otherwise noted, we set $Ca=10^5$. In the following, we also only focus on stability results for small to moderate bending modulus, which are limits closer to what could be expected in a physical system. We begin by investigating the small-wave number behavior of the linear stability in Sec. III A. We then investigate the linear electrohydrodynamic instability of a membrane with matching fluid viscosity and equal layer thickness: $\mu_r=1$ and $d_r=1$ in Sec. III B for a parallel electric field and Sec. III C for a normal electric field. We then study the effects of viscosity ratio in Sec. III D (with $d_r=1$), and the effect of layer thickness ratio in Sec. III E (with $\mu_r=1$).

## III. RESULTS

In the following, when a comparison is made with a fluid interface under an electric field, the membrane charging time is used to scale time in the fluid interface problem to be consistent with the formulation we have presented here for the capacitive IM/ES cases. For a capacitive elastic sheet with a large conductance and a small bending modulus ($g_m \gg 1$ and $\kappa \ll 1$), we expect the ES case to reduce to the problem of a fluid interface between two layers of leaky dielectric fluids. Therefore, we expect that the linear stability results for a capacitive ES with both $g_m \gg 1$ and $\kappa \ll 1$ to coincide with that for a fluid interface under an electric field. However, the electrohydrodynamic instability of a capacitive IM may be different due to the membrane incompressibility.

### A. Small wave number behavior

Here, we investigate the growth rate in the small wave number (long wavelength) limit for both the parallel and normal electric field cases. For a capacitive IM under a parallel electric field, the growth rate can be computed by expanding in small $k$ the quadratic equation (A1) given in the Appendix. Recall that in deriving this equation we neglected charge convection ($1/S \to 0$) and set $d_r = 1$. We find that one of the roots is always negative and is given by

$$\omega \approx -g_m - \left(\frac{5}{12} g_m + \frac{\sigma_r}{1+\sigma_r}\right) k^2 + \cdots. \tag{34}$$

The second root can either imply stability or instability and is given by

$$\omega \approx \frac{E_b(1-\sigma_r)(\varepsilon_r - 1)}{12(1+\sigma_r)(1+\mu_r)} k^2 \left(1 + mk^2 + \cdots\right), \tag{35}$$

where the coefficient $m$ of the quartic term is given by

$$m = \frac{2}{5} - \frac{2\sigma_r(\sigma_r + \varepsilon_r)}{g_m(1+\sigma_r)(1-\sigma_r)(1-\varepsilon_r)} - \frac{1}{Ca}\frac{1+\sigma_r}{E_b(1-\sigma_r)(1-\varepsilon_r)}. \tag{36}$$

Hence, a sufficient condition for instability of the IM case is $(1-\sigma_r)(\varepsilon_r - 1) > 0$ (so that the leading order term is positive). When $\mu_r = 1$, the growth rate for the IM and ES cases is identical and given by the formula in the Appendix. The above instability condition for a capacitive IM is identical to that for a fluid interface under a parallel electric field.[10–13] This is an interesting observation since it implies that the instability is driven by the electrical properties of the liquid and not by the properties of the membrane. Equation (35) shows that the growth rate $\omega$ is independent of $Ca$ at the leading order $O(k^2)$.

In deriving the above two growth rates, it was assumed that $g_m \neq 0$. Suppose now that the conductivity is zero, i.e., $g_m = 0$. A similar expansion in small $k$ of Eq. (A1) can be found and at leading order the two roots are proportional to $k^2$ and given by

$$\omega \approx k^2 \left(bc + dk^2 + \cdots\right), \tag{37}$$

where the coefficient $b$ is real and given by

$$b = -\frac{\sigma_r}{2(1+\sigma_r)} + \frac{E_b(1-\sigma_r)(\varepsilon_r - 1)}{24(1+\sigma_r)(1+\mu_r)}, \tag{38}$$

and the coefficient $c$ is complex in general and given by

$$c = 1 \pm \left[1 - \frac{E_b\sigma_r(\varepsilon_r + 1)}{12(1+\sigma_r)(1+\mu_r)b^2}\right]^{1/2}. \tag{39}$$

In the limit of $Ca \gg 1$, at leading order $O(Ca^{-1})$ both $b$ and $c$ are independent of $Ca$ while the coefficient $d$ depends on $Ca$ as

$$d = \frac{E_b(1-\sigma_r)(\varepsilon_r - 1)}{180(1+\sigma_r)(1+\mu_r)} + \frac{\sigma_r}{6(1+\sigma_r)} - \frac{1}{24(1+\mu_r)Ca} \pm \frac{1}{(1+\mu_r)(1+\sigma_r)}\left(\frac{f}{180} + \frac{g}{24Ca}\right), \tag{40}$$

where $f$ and $g$ are lengthy and complicated (and thus deferred to the Appendix). For the cases considered here, $c$ will be complex and a sufficient condition for instability will be determined by the sign of $b$, i.e., $b > 0$ implies long-wave instability. It is interesting to note that, unlike the nonzero conductivity case, the long-wave stability now depends on the magnitude of the initial tangential field and its relationship to the electrical properties of the liquids. In particular, this result implies that a zero membrane conductance ($g_m = 0$) can always be driven unstable ($b > 0$) at small wave numbers for a sufficiently strong tangential electric field and for $(1 - \sigma_r)(\varepsilon_r - 1) > 0$, which is the instability condition for a conducting membrane ($g_m > 0$) under a parallel electric field. Thus, the long-wave expansions imply that it is possible for the condition of instability for a conducting membrane to be met, and for a non-conducting membrane to still be stable. This suggests a more careful investigation of the effect of $g_m$ on instability is warranted, and will be provided in Sec. III B (Figure 7).

For a capacitive IM under a normal electric field, the membrane conductance is essential to the electrohydrodynamic instability as the condition for instability is $g_m(\sigma_r - 1)(\sigma_r^2 - \varepsilon_r) > 0$ (see Refs. 15, 17, and 19). In the long-wave ($k \to 0$) limit, the real part of the linear growth rate for a flat membrane under a normal electric field is found to be[15]

$$\Re(\omega) \approx \frac{E_b g_m^3 (\sigma_r - 1)\left(\sigma_r^2 - \varepsilon_r\right)}{96(1 + \mu_r)[1 + (\sigma_r + 1)g_m/2]^3} k^2 - \frac{\kappa}{96(1 + \mu_r)} k^6, \tag{41}$$

consistent with the above noted instability condition. This instability condition is identical to that for a fluid interface under a background Poiseuille flow,[10–13] but the details of the dispersion relation are different.[11] Hence, as with the parallel electric field case, instability depends on the electrical properties of the liquids (assuming $g_m \neq 0$), but unlike the parallel field case, the membrane is stable if $g_m = 0$.[16]

### B. Parallel electric field with $d_r = 1$ and $\mu_r = 1$

As noted earlier, the growth rate is identical for both IM and ES for $1/S \to 0$, $d_r = 1$, and $\mu_r = 1$. Hence we will not discuss the ES case, and will focus on IM with $S \ll 1$. As suggested in Eq. (41), the bending force is always stabilizing in the linear regime. Therefore, we begin by first focusing on the $\kappa = 10^{-6}$ case for a capacitive IM under a parallel electric field. In Figure 2, we show the growth rate as a function of wave number $k$ for the two sets of parameters with $\sigma_r \leq 1$ from Figure 3 in Ref. 13 to make comparison and connection to the case of a fluid interface under an electric field. The dashed curves in Figure 2 are for a fluid interface. For a non-conducting membrane ($g_m = 0$), the membrane is stable in panel (a) where $\varepsilon_r = 2$ and $\sigma_r = 0.5$, while for panel (b) where $\varepsilon_r = 2$ and $\sigma_r = 0.2$ the non-conducting membrane is unstable. This is consistent with Eq. (37) with $c$ complex and $b = -7/3 < 0$ (stable) for Figure 2(a) while $b = 16/15 > 0$ (unstable)

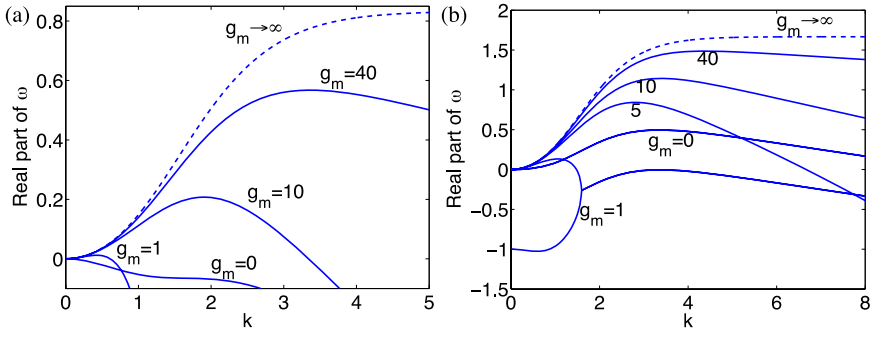


FIG. 2. Comparison of the growth rate magnitude for the parallel electric field. $E_b = 10$, $Ca = 10^5$, $S = 10^6$, and $\kappa = 10^{-6}$. (a) $\varepsilon_r = 2$, $\sigma_r = 0.5$. (b) $\varepsilon_r = 2$, $\sigma_r = 0.2$. Dashed curves are for the fluid interface ($g_m \to \infty$). Solid lines are for the capacitive membrane for five values of $g_m$: 0, 1, 5, 10, and 40.

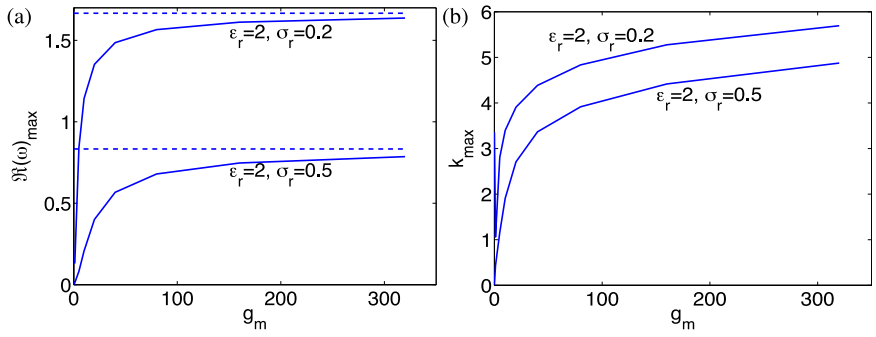


FIG. 3. Maximum growth rate $\Re(\omega)$ and $k_{\max}$ versus the membrane conductance $g_m$ for the parallel electric field cases in Figure 2 with $g_m > 0$. The dashed curves correspond to values for a fluid interface with the same physical parameters in the bulk.

for Figure 2(b). As noted earlier, this means that an electric field tangent to a capacitive membrane can destabilize the membrane with zero conductance and that the dominant unstable mode is oscillatory for $g_m = 0$ ($\omega$ has a non-zero imaginary part). As indicated in the figure, this dominant oscillatory mode for $g_m = 0$ is replaced by a steady mode for $g_m > 0$. Figure 2(b) also illustrates that, for $g_m > 5$, the dominant steady mode moves to higher $k_{\max}$ as membrane conductance $g_m$ increases and eventually the growth rate approaches that of the fluid interface as $g_m \to \infty$. This is further illustrated in Figure 3, where the maximum growth rate and maximum wave number are plotted for the cases in Figure 2 as a function of $g_m$. These results show that $g_m \sim O(100)$ is sufficient to reach the values for a conducting fluid interface. The limiting unstable growth rate as $g_m \to \infty$ can be explicitly found from Eq. (A1) and is given by

$$\omega = \frac{(k^2 - \sinh^2 k)}{2(1+\mu_r)}\left[\frac{k\sinh k(1+\sigma_r)(\frac{1}{Ca}+\kappa k^2) + E_b \cosh k(1-\sigma_r)(1-\varepsilon_r)}{(1+\sigma_r)\sinh k(k+\sinh k\cosh k)}\right]. \tag{42}$$

Note that sending $g_m$ to infinity does not change the instability criterion which is given by the term containing $E_b$ in Eq. (42). Comparing this linear growth rate to those from Eq. (51) in Ref. 13, we find agreement with their growth rates in their Figure (3) provided that $A_{2p}$ in their Eq. (50) is divided by $k$.

In Figure 4, we examine the effects of the membrane bending modulus $\kappa$. As expected, $\kappa$ is stabilizing, in that the growth rate should decrease as $\kappa$ increases. This is illustrated for both of the cases in Figure 2 in that the growth rate and the maximum wave number decrease with $\kappa$.

The effects of $S$ and $Ca$ on the growth rate for parameters in Figure 2(b) are plotted in Figure 5 for $g_m = 0$. It should be noted that both ES/IM are solved for parameters in Figure 5 and the results are indistinguishable. Therefore, we do not distinguish these two cases in the following discussion.

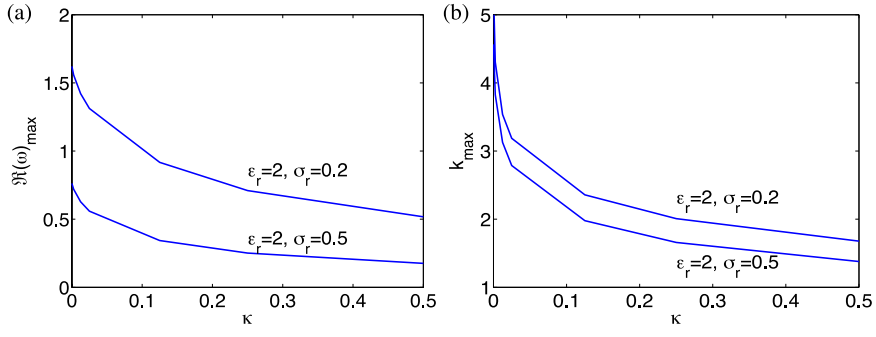


FIG. 4. Maximum growth rate $\Re(\omega)$ and $k_{\max}$ versus the membrane bending modulus $\kappa$ for the parallel electric field cases in Figure 2 with $g_m = 200$.

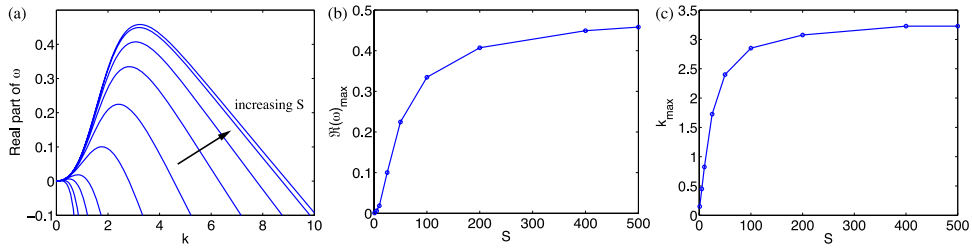


FIG. 5. Effects of $S$ with $g_m = 0$, $Ca = 10^3$, $\kappa = 10^{-6}$, $\varepsilon_r = 2$, and $\sigma_r = 0.2$. (a) Growth rate at different values of $S$. (b) Maximum growth rate versus $S$. (c) Maximum wave number versus $S$.

Figure 5(a) shows the growth rate at different values of $S$ with small surface tension ($Ca \gg 1$). As $S$ increases from 1 to 500, the maximum growth rate increases and reaches the maximum value at $S \to \infty$. Figure 5(b) explicitly plots the maximum value of the growth rate versus $S$ showing the monotonic increase and similarly in Figure 5(c), the monotonic increase in the maximum wave number with $S$ is plotted. Figure 6 shows the dependence of capillary number $Ca$ with $S = 500$, and it is clear that both the maximum growth rate and the maximum wave number plateau for $Ca \geq 100$.

Figure 6(a) shows that for large $Ca$, the growth rate at small wave numbers is insensitive to $Ca$, which can be explained by Eq. (35) where the leading order growth rate is independent of $Ca$ at small wave numbers. As $Ca$ increases, the critical cutoff wave number $k_c$ for instability plateaus around 9, also independent of $Ca$ as we concluded in the paragraph right below Eq. (35) in Sec. III A. The expected values of both $Ca$ and $S$ are large in problems of biological interest and these plots illustrate that a reasonable approximation is to neglect the effect of $S$ and $Ca$ in discussing the instability of the membrane.

Neglecting the effect of charge convection on the membrane (by setting $S \gg 1$ such that $1/S \to 0$) allows us to identify a sufficient condition for instability directly from the small $k$ expansions. As noted earlier, for a conducting membrane if $(1 - \sigma_r)(\varepsilon_r - 1) > 0$, then the membrane is unstable. For a nonconducting membrane ($g_m = 0$), we find from Eqs. (37) and (38) that the interface is stable for $k \ll 1$ if $\varepsilon_r < 1$ and $\sigma_r < 1$. For $\varepsilon_r > 1$, the long-wave instability can occur when

$$\sigma_r < \frac{E_b\,(\varepsilon_r - 1)}{48/(1 + \mu_r) + E_b(\varepsilon_r - 1)} \equiv \sigma_r^l. \tag{43}$$

Note this implies that the stability boundary starts at $\sigma_r = 0$ for $\varepsilon_r = 1$ and then monotonically increases to 1 as $\varepsilon_r$ increases. Our computations show a similar behavior for finite values of $S$.

Equation (43) is a sufficient (but not necessary) condition for instability. Computations show that, if $\sigma_r > \sigma_r^l$, the instability can still occur at a finite-wave number even though the growth rate is negative around $k = 0$. Figures 7(a) and 7(b) show that, for $g_m = 0$ and $\sigma_r = 0.41$ ($> \sigma_r^l = 0.29$ for parameters provided in Figure 7), the growth rate is negative at small wave number and yet a positive growth rate is found for a window around $k \sim 2.3$. For $g_m = 0$ the growth rate is a complex pair along the dashed curves in (a) and (b). For $g_m > 0$, a local maximum (corresponding to a real growth rate) emerges from small $k$, and the two real growth rates (at small wave numbers) collide

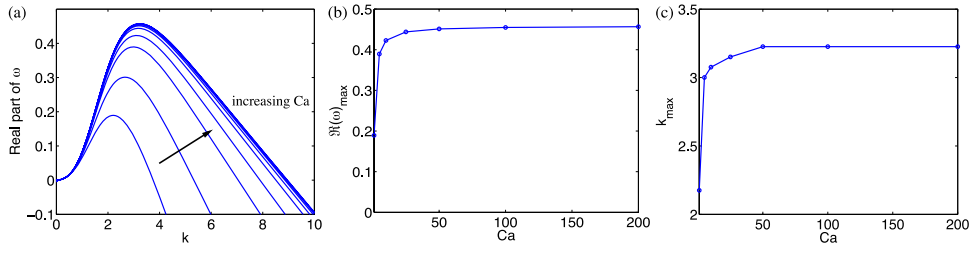


FIG. 6. Effects of $Ca$ with $g_m = 0$, $S = 500$, $\kappa = 10^{-6}$, $\varepsilon_r = 2$, and $\sigma_r = 0.2$. (a) Growth rate at different values of $Ca$. (b) Maximum growth rate versus $Ca$. (c) Maximum wave number versus $Ca$.

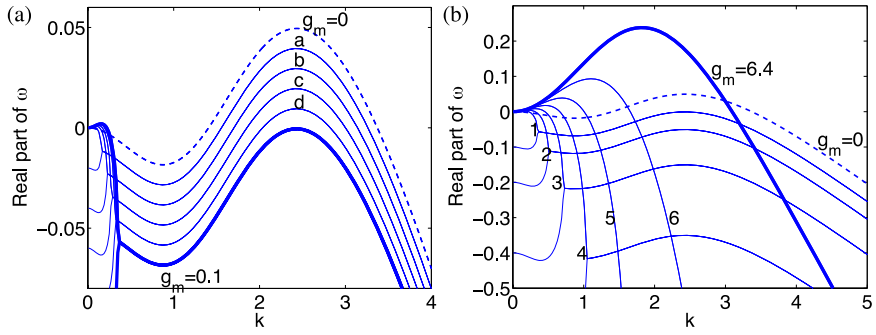


FIG. 7. Growth rate for $\sigma_r > \sigma_r^l$ (defined in Eq. (43)). $Ca = 10^5$, $S = 10^5$, $\kappa = 10^{-6}$, $E_b = 10$, $\varepsilon_r = 2$, $\sigma_r = 0.41 > \sigma_r^l = 0.29$. (a) Growth rate for small membrane conductance: $g_m = 0.01$, 0.02, 0.04, and 0.08 for curves a, b, c, and d, respectively. (b) Growth rate for moderate membrane conductance: $g_m = 0.1$, 0.2, 0.4, 0.8, 1.6, and 3.2 for curves 1 to 6, respectively.

to a complex pair as shown in Figure 7. We also observe that, as $g_m$ increases, the real part of the complex pair around $k \sim 2.3$ decreases and the maximum growth rate becomes real for $g_m \geq 0.1$, replacing the complex maximum growth rate for $g_m \leq 0.08$. From the computations, we find the conducting membrane is always unstable for $(1 - \sigma_r)(\varepsilon_r - 1) > 0$, consistent with the long-wave analysis. For the non-conducting membrane, the instability boundary depends on both $S$ and $E_b$ (see Eq. (43) for $1/S = 0$). Figure 8 shows the instability boundary for a non-conducting ($g_m = 0$) capacitive IM for $S = 100$ (dash-dotted curves) and $1/S = 0$ for negligible charge convection (solid curves) at different values of electric field strength $E_b$: $E_b = 62.5$, 250, and 1000 for curves 1, 2, and 3. Values of $\sigma_r$ greater than 1 are plotted in Figure 8 even though we earlier stated that because of the symmetry of the parallel field case we would only consider $\sigma_r < 1$. This is done to illustrate that in our dimensionless scaling (based on fluid 2), the stability boundaries are asymmetric between the two unstable quadrants in Figure 8.

### C. Normal electric field with $d_r = 1$ and $\mu_r = 1$

In electroformation experiments, both AC and DC electric fields perpendicular to the planar membrane are employed to drive the membrane unstable to form vesicles. A Floquet linear analysis for a tensionless membrane under an AC electric field in an infinite domain shows that an elastic capacitive membrane (with or without membrane conductance) can be unstable for small wave

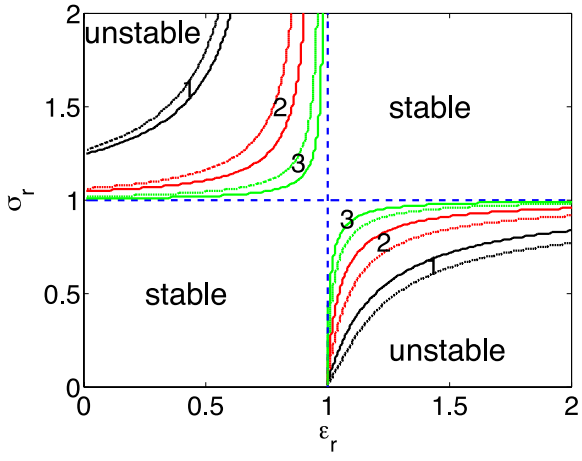


FIG. 8. Boundary of instability in the $(\varepsilon_r, \sigma_r)$ plane for a capacitive membrane under a parallel electric field. The dashed (blue) curves are the stability boundaries $\varepsilon_r = 1$ and $\sigma_r = 1$ for $g_m > 0$. For $g_m = 0$, the stability boundary depends on $S$ and $E_b$: $E_b = 62.5$, 250, and 1000 for curves 1 (black), 2 (red), and 3 (green) with $Ca = 10^5$, and $\kappa = 10^{-6}$. $S = 100$ for the dash-dotted curves. Solid curves are for negligible charge convection ($1/S = 0$).

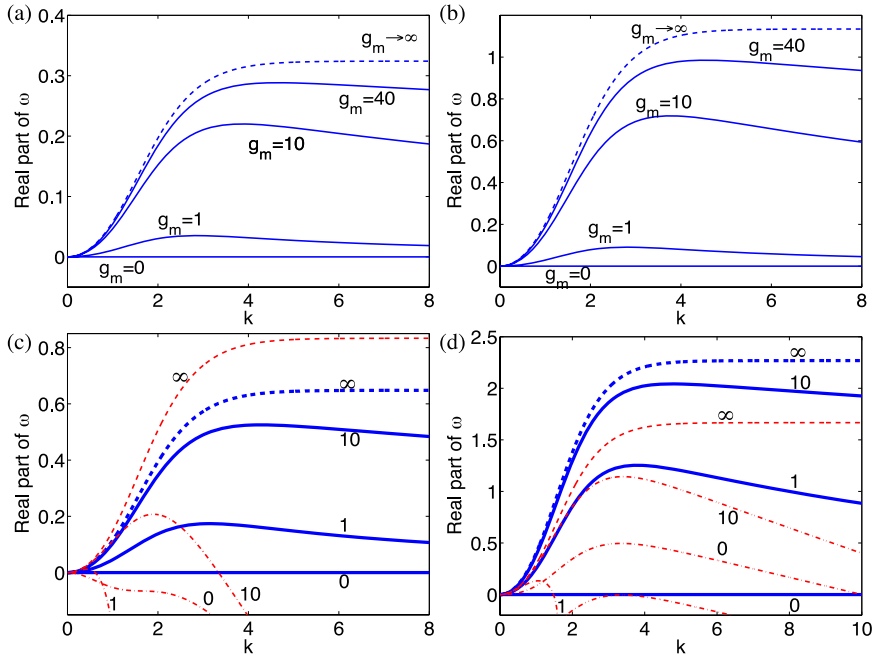


FIG. 9. Comparison of the growth rate magnitude for the normal electric field. $S = 10^6$, $Ca = 10^5$, $\kappa = 10^{-6}$, and $E_b = 10$. (a) $\varepsilon_r = 0.5$, $\sigma_r = 2$. (b) $\varepsilon_r = 0.5$, $\sigma_r = 5$. (c) $\varepsilon_r = 2$, $\sigma_r = 0.5$. (d) $\varepsilon_r = 2$, $\sigma_r = 0.2$. Dashed curves are for the fluid interface ($g_m \to \infty$). Solid (blue) lines are for the capacitive membrane with $\kappa = 10^{-6}$ and three values of $g_m$: 0, 1, and 10. Thin (red) curves are from Figure 2.

numbers at small-to-moderate AC field frequencies.[19] A long-wave analysis for a membrane under a normal electric field in a finite domain was conducted in Ref. 15, and the linear stability of a planar membrane in a DC normal electric field was investigated in Refs. 16 and 17. Here, we focus on a DC electric field perpendicular to a flat planar membrane in a finite channel without the long-wave assumption. As in the parallel field case, both the incompressible membrane and the elastic sheet give the same linear stability results when $d_r = 1$ and $\mu_r = 1$.

Results from our calculations confirm that the capacitive IM under a normal electric field is stable when the membrane conductance $g_m = 0$.[16] Figure 9 shows the dependence of the growth rate on membrane conductance with $\kappa = 10^{-6}$. Figures 9(a) and 9(b) are for $\sigma_r > 1$, and (c) and (d) are for the parameters from Figure 2. For comparison, the results for the parallel cases in Figure 2 are also included in 9(c) and 9(d) (thin dashed lines and dash-dotted lines). Unlike in the parallel electric field case, the membrane conductance has to be positive for a capacitive IM/ES to be

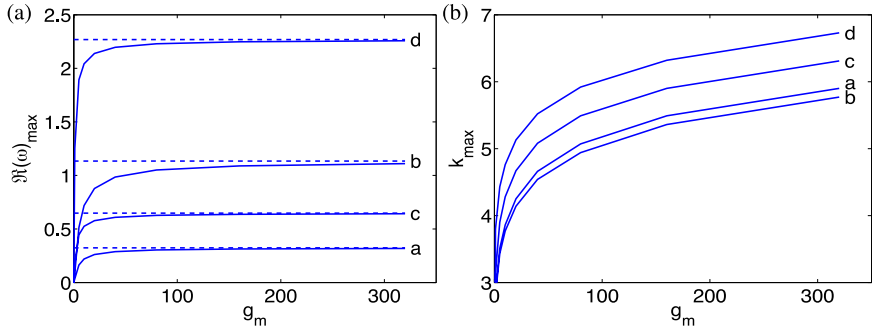


FIG. 10. Maximum growth rate $\Re(\omega)$ and $k_{\max}$ versus the membrane conductance $g_m$ for the four normal electric field cases (as labeled) in Figure 9. The dashed curves in (a) correspond to values for a fluid interface with the same physical parameters in the bulk. $S = 10^6$, $Ca = 10^5$, $\kappa = 10^{-6}$, and $E_b = 10$. For the four curves labeled a, b, c, d, $(\varepsilon_r, \sigma_r) = (0.5, 2)$, $(0.5, 5)$, $(2, 0.5)$, and $(2, 0.2)$, respectively.

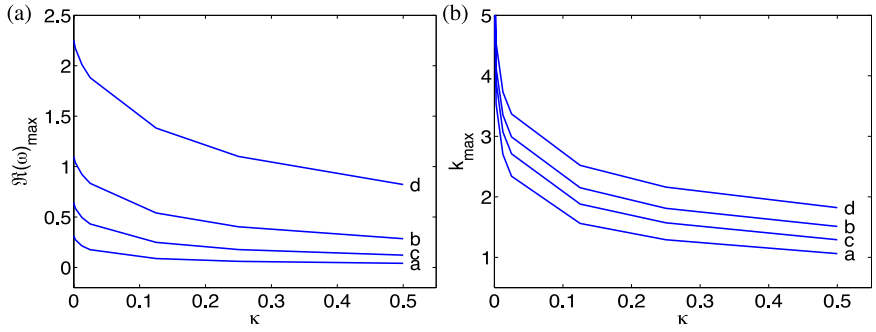


FIG. 11. Maximum growth rate $\Re(\omega)$ and $k_{\max}$ versus the membrane bending modulus $\kappa$ for the four normal electric field cases (as labeled) in Figure 9. $S = 10^6$, $Ca = 10^5$, $\kappa = 10^{-6}$, $E_b = 10$, and $g_m = 200$. For the four curves labeled a, b, c, d, $(\varepsilon_r, \sigma_r) = (0.5, 2)$, $(0.5, 5)$, $(2, 0.5)$, and $(2, 0.2)$, respectively.

unstable under a normal electric field. For all four cases in Figure 9, the growth rate approaches that for a fluid interface (blue dashed curves) as $g_m \to \infty$. For membrane conductance, $g_m = 0$, 1, and 10 in Figure 9(c), the maximum wave number $k_{\max}$ for the parallel cases is smaller than for the normal cases. Figure 9(d) shows that, except for $g_m = 0$, the normal electric field (thick curves) is more destabilizing than the parallel electric field (thin curves): For $g_m \geq 1$, the growth rates for a normal electric field are larger than for a parallel electric field. Interestingly, in (c) the parallel electric field gives larger growth rates for the fluid interface case ($g_m \to \infty$) while for conducting IM the normal electric field again gives larger growth rates.

Figure 10 shows the $g_m$-dependence of the maximum growth rate and $k_{\max}$ for Figure 9. We find that the maximum growth rate is always positive for $g_m > 0$. The dashed curves correspond to the values of the maximum growth rate for a fluid interface ($g_m \to \infty$). Similar to the results for the parallel electric field case in Figure 3, the maximum growth rate plateaus around $g_m \geq 100$ in these parameter ranges. Figure 11 shows the dependence of the maximum growth rate and $k_{\max}$ on the membrane bending modulus. The maximum growth rate is almost independent of $\kappa$ for cases (a) and (c) in Figure 11(a), while $k_{\max}$ decreases slightly with $\kappa$ for these two cases in Figure 11(b).

For a capacitive IM perpendicular to the electric field, the growth rate from Eq. (41) shows that either membrane tension or the bending force is needed to stabilize the membrane at high wave numbers. Figure 12(a) shows the growth rate for various values of the capillary number with $\kappa = 10^{-6}$, which gives rise to damping at large wave numbers and consequently a large critical wave number. As $Ca$ increases from 1 to 100, the maximum growth rate plateaus around $Ca \sim 100$ as shown in Figure 12(b) while $k_{\max}$ in Figure 12(c) increases gradually with $Ca$.

Figure 13(a) shows the dependence of the growth rate on $S$ with $g_m = 200$ and $Ca = 10^3$ under a normal electric field. Results in (a) show that the growth rate plateaus to the maximum value at large wave number because $Ca = 10^3 \gg 1$. Compared against the parallel case in Figure 5(a), we observe that the perturbation at $k \gg 1$ is hardly damped under a normal electric field with $Ca = 10^3$, while for a parallel electric field the perturbation at large $k$ is stable. For this set of parameters, the maximum growth rate increases with $S$ for both parallel and normal electric fields.

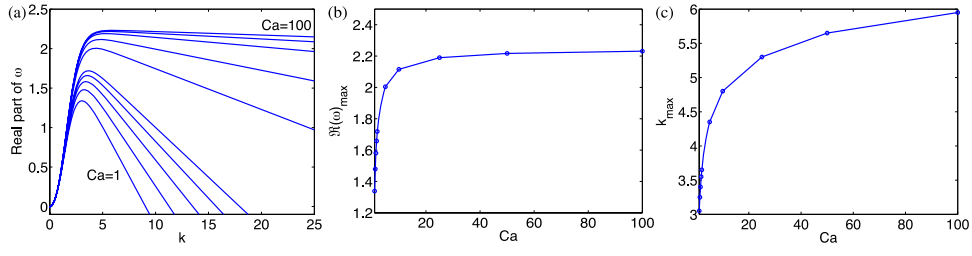


FIG. 12. Effects of $Ca$ with $S = 500$, $g_m = 200$, $\kappa = 10^{-6}$, $\varepsilon_r = 2$ and $\sigma_r = 0.2$ with a normal electric field. (a) Growth rate at different values of $Ca$. (b) Maximum growth rate versus $Ca$. (c) $k_{\max}$ versus $Ca$.

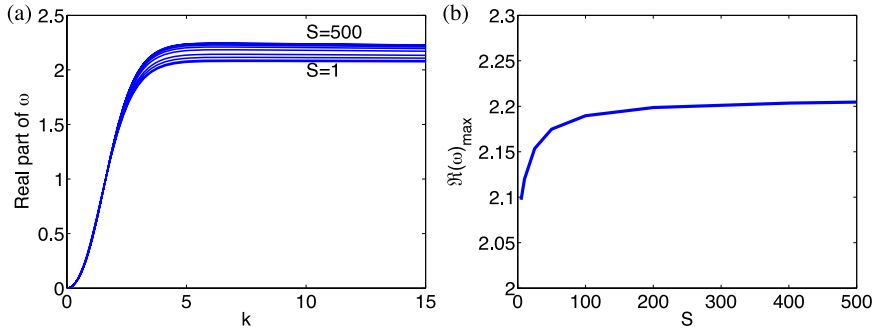


FIG. 13. Effects of $S$ with $Ca = 10^3$, $g_m = 200$, $\kappa = 10^{-6}$, $\varepsilon_r = 2$, and $\sigma_r = 0.2$ with a normal electric field. (a) Growth rate at different values of $S$. (b) Critical wave number versus $S$.

Figure 14 shows the regions of instability for $Ca = 10^3 \gg 1$, $g_m = 1$, and $\kappa = 10^{-3}$. Figure 14(a) illustrates the dependence of instability boundary on $S$ with $E_b = 1$: For $S \geq 0.1$, the stability boundaries are $\sigma_r = 1$ and $\sigma_r = \sqrt{\varepsilon_r}$, denoted by the solid curves. For $S = 0.01$, the stability region shrinks. For example, for $E_b = 1$, the stable region is bounded by $\sigma_r = 1$, $\sigma_r = \sqrt{\epsilon_r}$, and the curve 1. The inset shows the stability boundary for $E_b = 16$, 32, and 64 (curves 5, 6, and 7, respectively). Note that as in Figure 8, because of the characteristic scaling based on fluid 2, symmetry about the lines $\sigma_r = 1$ and $\epsilon_r = 1$ cannot be expected if $\sigma_r$ and $\epsilon_r$ are replaced by their inverses.

In the $(\varepsilon_r, \sigma_r)$ plane where both parallel and normal electric fields can destabilize a fluid interface, sub-regions of instability dominated by either parallel or normal field are identified in Refs. 12 and 13 for a fluid interface. For a capacitive IM, this dominance is dependent on the membrane conductance. Consider the case where, with $g_m = 0$, a parallel electric field can drive an IM unstable in regions of the quadrant $\sigma_r < 1$ and $\varepsilon_r > 1$ as shown in Figure 8. But a normal electric field cannot destabilize a non-conducting membrane as shown in Figures 9 and 10, where the growth rate is zero when $g_m = 0$. From Figure 9(d), we see that the reverse is true when $g_m \geq 1$, where a larger growth rate is found for the normal electric field.

### D. Effect of viscosity ratio $\mu_r$ with $d_r = 1$

For matching fluid viscosity ($\mu_r = 1$) and layer thickness ($d_r = 1$), we found that the stability of IM and ES is identical. This is no longer the case when $\mu_r \neq 1$. An analytical formula for the growth rate in the parallel field IM case (with arbitrary $\mu_r$) is given in the Appendix but only computational results will be presented for all other cases. To illustrate the effect of viscosity contrast, here we fix $\mu_r = 2$ and compare the maximum growth rate between a capacitive IM (solid curves) and a capacitive ES (dashed curves) in Figure 15 for a parallel electric field. In Figure 15, we plot the

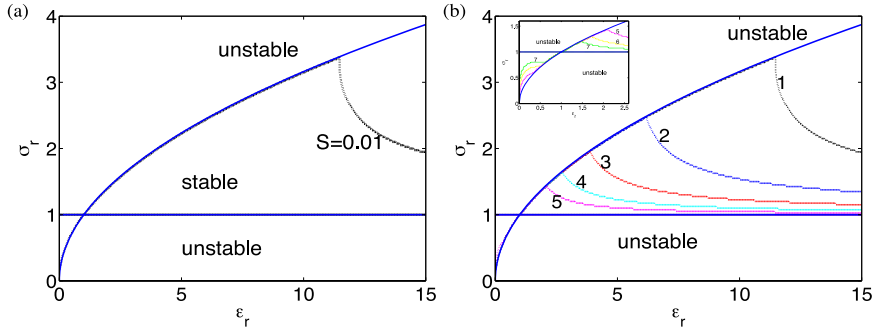


FIG. 14. Boundary of instability in the $(\varepsilon_r, \sigma_r)$ plane for a capacitive IM under a normal electric field for $Ca = 10^3$, $\kappa = 10^{-3}$, and $g_m = 1$. Solid curves are $\sigma_r = 1$ and $\sigma_r = \sqrt{\varepsilon_r}$, the stability boundaries for $S \geq 0.1$, independent of electric field strength $E_b$. (a) Dependence on $S$ with $E_b = 1$. (b) Dependence on $E_b$ with $S = 0.01$. $E_b = 1$, 2, 4, 8, and 16 for curves 1, 2, 3, 4, and 5, respectively. In the inset, $E_b = 16$, 32, and 64 for curves 5, 6, and 7, respectively.

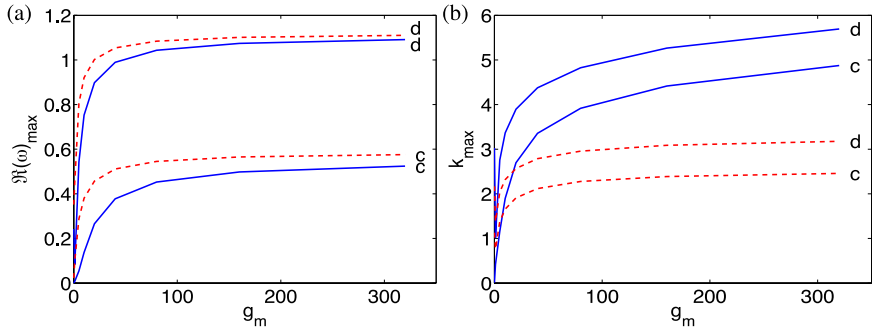


FIG. 15. Maximum growth rate (panel (a)) and wave number (panel (b)) versus $g_m$ for a parallel electric field with $S = 10^6$, $Ca = 10^5$, and $\kappa = 10^{-6}$. Solid curves are for an IM and dashed curves are for an ES. (c) $\varepsilon_r = 2$, $\sigma_r = 0.5$. (d) $\varepsilon_r = 2$, $\sigma_r = 0.2$.

maximum growth rate in panel (a) and $k_{\max}$ in panel (b) for the two cases in Figure 2 under a parallel electric field. Smaller growth rates are found for the capacitive IM (solid curves), while larger $k_{\max}$ is found in panel (b). Figure 16 shows the comparison for a capacitive IM/ES under a normal electric field with parameters for the four cases in Figure 9. Except for case (a), we find that the maximum growth rate and $k_{\max}$ behave similarly between an IM and an ES under a normal electric field. From these results, we observe that dynamics of the IM/ES cases can differ more significantly with $\mu_r$ under a parallel electric field than a normal electric field.

### E. Effect of layer thickness ratio $d_r$ with $\mu_r = 1$

The linear stability of a planar shear flow in a two-layer system depends on the ratio of layer thickness.[9,21] Here, we illustrate that $d_r$ also affects the electrohydrodynamic instability shown in Secs. III B and III C. Figure 17 shows how the maximum growth rate for a capacitive IM varies with $d_r$ for the two cases in Figure 2. Under a parallel electric field, a non-conducting ($g_m = 0$) membrane is stable in panel (a) while the membrane can become unstable (dash-dotted curve) in Figure 2(b). In panel (a), the maximum growth rate increases with both $g_m$ and $d_r$, while in panel (b) we find that a conducting membrane with an intermediate membrane conductance ($g_m = 2$) can become linearly stable for large values of $d_r$ ($d_r > 1.25$). At large membrane conductance, however, the membrane is unstable for $0.4 \le d_r \le 1.5$ in both panels.

Figure 18 shows the effects of $d_r$ for a capacitive IM under a normal electric field, where membrane conductance is essential for the electrohydrodynamic instability. For $g_m = 1$, an optimal layer thickness ratio is found to be in the range $0.5 \le d_r \le 1$. Apparently, such optimal layer thickness ratio for instability depends on the mismatch in electric permittivity and conductivity. As the membrane conductance increases to $g_m = 10$ the optimal layer thickness ratio decreases. For $g_m \ge 100$, we find that the maximum growth rate decreases with $d_r$ in both panels.

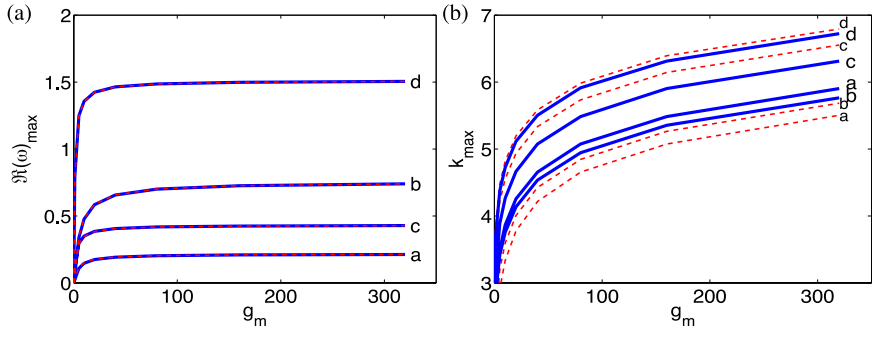


FIG. 16. Maximum growth rate (panel (a)) and wave number (panel (b)) versus $g_m$ for a perpendicular electric field with $S = 10^6$, $Ca = 10^5$ and $\kappa = 10^{-6}$. Solid curves are for an incompressible membrane and dashed curves are for an elastic sheet. (a) $\varepsilon_r = 0.5$, $\sigma_r = 2$. (b) $\varepsilon_r = 0.5$, $\sigma_r = 5$. (c) $\varepsilon_r = 2$, $\sigma_r = 0.5$. (d) $\varepsilon_r = 2$, $\sigma_r = 0.2$.

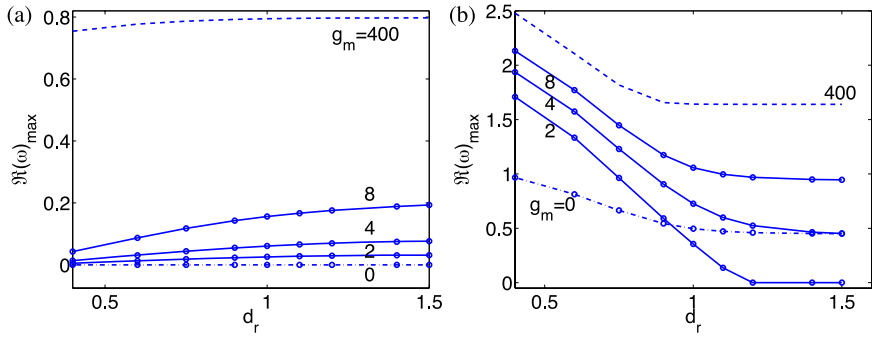


FIG. 17. Maximum growth rate versus $d_r$ for a parallel electric field with $S = 10^6$, $Ca = 10^5$, $\kappa = 10^{-6}$, and different values of membrane conductance as labeled. (a) $\varepsilon_r = 2$, $\sigma_r = 0.5$. (b) $\varepsilon_r = 2$, $\sigma_r = 0.2$.

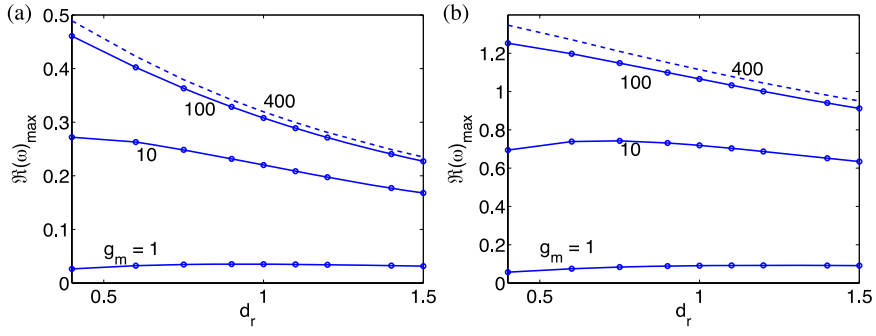


FIG. 18. Maximum growth rate versus $d_r$ for a normal electric field with $S = 10^6$, $Ca = 10^5$, $\kappa = 10^{-6}$, and different values of membrane conductance as labeled. (a) $\varepsilon_r = 0.5$, $\sigma_r = 2$. (b) $\varepsilon_r = 0.5$, $\sigma_r = 5$.

## IV. CONCLUSION

In this work, the electrohydrodynamic instability of an elastic capacitive membrane immersed in leaky dielectric fluids in a channel is investigated, with focuses on physically relevant parameters: $Ca \gg 1$, $\kappa \ll 1$, and $S \gg 1$. Although this investigation was done in two-dimensions, experimental results for the electrohydrodynamic instability of a fluid interface under shear flow[1] suggest that the two-dimensional linear dynamics is the dominant initial instability. This observation lends support to our investigation. When the membrane is parallel to the electric field, it is found that the parallel electric field stabilizes the high wave number perturbations. At low wave numbers, a non-conducting capacitive membrane may be unstable according to Eq. (43), which is a sufficient condition for instability. Interestingly, we find that a capacitive IM under a parallel electric field can be unstable in a window about a finite wave number while stable about $k = 0$ (Figure 7). Furthermore, we show how the stability boundary depends on the electric field strength $E_b$ for a non-conducting IM under a parallel electric field in Figure 8. When the imposed electric field is normal to the membrane, regions of linear instability are found to depend on the charge relaxation time (Figure 14): Smaller regions for linear stability are found for $S < 0.1$, while for $S \geq 1$ the regions of linear instability are identical to those for a fluid interface under a normal electric field.

In addition, effects of the membrane conductance ($g_m$), tension ($Ca$), and membrane bending forces ($\kappa$) on the electrohydrodynamic instability are quantified in this work. The effect of charge convection, $S$, (the ratio of bulk charging time to membrane charging time) is also explored. It is found that the membrane is more unstable for large $S$ (small charge convection) under a parallel electric field, while $S$ tends to stabilize the membrane under a perpendicular electric field.

The effects of viscosity ratio ($\mu_r$) and layer thickness ratio ($d_r$) on the electrohydrodynamic instability are investigated for a few cases. These results illustrate that an incompressible lipid bilayer membrane behaves as an ES under an electric field (both parallel and normal) when $\mu_r = 1$

and $d_r = 1$. In addition, for the few cases that we discuss in Sec. III E, there exists an optimal layer thickness ratio for the instability of an elastic membrane under a normal electric field.

Normal electric fields are employed more often in experiments because they are easier to set-up compared to tangential fields. Yet, our results here imply that in certain circumstances, an electric field parallel to the interface might be more beneficial. Both AC and EC normal electric fields have been extensively studied theoretically, and a long-wave investigation on a fluid interface under a normal AC field showed pillar formation as a nonlinear consequence of the linear instability.[22,23] From electroformation experiments it is speculated that the linear electrohydrodynamic instability of a membrane under a normal electric field may lead to vesicle formation, and yet a long-wave investigation of this system shows evidence that more physics is required to fully understand the electroformation experiments. Results from this work lay the foundation for incorporating more physics such as ionic solvents to replace the leaky dielectric fluids. For example, the pH values of the solvents are known to affect the lipid membrane stability.[24] We are now investigating how the electrohydrodynamic instability reported in this work might be affected by the pH values of solvents.

## ACKNOWLEDGMENTS

The authors acknowledge helpful comments from the referees. Y.N.Y. acknowledges useful discussions with P. Vlahovska, and support from NSF under Grant No. DMS-1222550. M.J.M. acknowledges support from NSF Grant No. DMS-1312935.

## APPENDIX: GROWTH RATE FOR AN INCOMPRESSIBLE MEMBRANE IN A PARALLEL ELECTRIC FIELD WITH $1/S = 0$

The growth rate $\omega$ for a capacitive IM in a parallel electric field with zero charge convection along the interface ($1/S = 0$) and $d_r = 1$ satisfies the following (dimensionless) quadratic equation:

$$A_2\omega^2 + A_1\omega + A_0 = 0. \tag{A1}$$

The variables $A_0$, $A_1$, and $A_2$ depend on all the electrical properties and are given by

$$A_2 = -2(1+\mu_r)(1+\sigma_r)k\cosh k\,(k+\cosh k\sinh k),$$
$$A_1 = g_m A_2 - B_1 - 2k^2\sigma_r(1+\mu_r)\sinh k\,(k+\cosh k\sinh k),$$
$$A_0 = -g_m B_1 - k^2\sigma_r\left(\sinh^2 k - k^2\right)\left[E_b\left(\varepsilon_r+1\right)\cosh k + k\sinh k\left(\frac{1}{Ca}+\kappa k^2\right)\right],$$
$$B_1 = k\cosh k\left(\sinh^2 k - k^2\right)\left[E_b(1-\sigma_r)(1-\epsilon_r)\coth k + k(1+\sigma_r)\left(\frac{1}{Ca}+\kappa k^2\right)\right].$$

It is interesting to note that when viscosity ratio is one, i.e., $\mu_r = 1$, the growth rate for the incompressible membrane and the elastic sheet problem is identical in a parallel electric field.

The expressions for $f$ and $g$ in Sec. III A are

$$f = \frac{E_b^2(1-\sigma_r)^2(\varepsilon_r-1)^2 - 360(1+\mu_r)^2\sigma_r^2 + 18E_b(1+\mu_r)\sigma_r(1+3\sigma_r+\varepsilon_r(3+\sigma_r))}{\sqrt{-48E_b(1+\mu_r)(\varepsilon_r+1)\sigma_r(1+\sigma_r)+(E_b(\varepsilon_r-1)(-1+\sigma_r)+12(1+\mu_r)\sigma_r)^2}}, \tag{A2}$$

$$g = \frac{(1+\sigma_r)(E_b(\varepsilon_r-1)(-1+\sigma_r)-12(1+\mu_r)\sigma_r)}{\sqrt{E_b^2(\varepsilon_r-1)^2(-1+\sigma_r)^2+144(1+\mu_r)^2\sigma_r^2-24E_b(1+\mu_r)\sigma_r(1+3\sigma_r+\varepsilon_r(3+\sigma_r))}}. \tag{A3}$$

[1] O. Ozen, N. Aubry, D. T. Papageorgiou, and P. G. Petropoulos, "Monodisperse drop formation in square microchannels," Phys. Rev. Lett. **96**, 144501 (2006).
[2] N. Wu and W. B. Russel, "Micro- and nano-patterns created via electrohydrodynamic instability," Nano Today **4**, 180–192 (2009).
[3] L. Haiwang, W. T. Neng, and N. Name-Trung, "Electrohydrodynamic and shear-stress interfacial instability of two streaming viscous liquid inside a microchannel for tangential electric field," Micro Nanosyst. **4**, 14 (2012).
[4] P. Sharifi and A. Esmaeeli, "Comparison of EHD-driven instability of thick and thin liquid films by a transverse electric field," Fluid Dyn. Mater. Process. **9**, 389 (2013).

[5] M. I. Angelova and D. S. Dimitrov, "Liposome electroformation," Faraday Discuss. Chem. Soc. **81**, 303–311 (1986).
[6] M. I. Angelava and D. S. Dimitrov, "Swelling of charged lipids and formation of liposomes on electrode surfaces," Mol. Cryst. Liq. Cryst. Incorporating Nonlinear Opt. **152**, 89–104 (1987).
[7] M. I. Angelova, S. Soleau, Ph. Meleard, J. F. Faucon, and P. Botheorel, "Preparation of giant vesicles by external ac electric fields. Kinetics and applications," Prog. Colloid Polym. Sci. **89**, 127–131 (1992).
[8] D. van Swaay and A. deMello, "Microfluidic methods for forming liposomes," Lab Chip **13**, 752 (2013).
[9] S. G. Yiantsios and B. G. Higgins, "Linear stability of plane Poiseuille flow of two superposed fluids," Phys. Fluids **31**, 3225 (1988).
[10] O. Ozen, N. Aubry, D. T. Papageorgiou, and P. G. Petropoulos, "Electrohydrodynami linear stability of two immiscielbe fluids in channel flow," Electrochim. Acta **51**, 5316–5323 (2006).
[11] F. Li, O. Ozen, N. Aubry, D. T. Papageorgiou, and P. G. Petropoulos, "Linear stability of a two-fluid interface for electrohydrodynamic mixing in a channel," J. Fluid Mech. **583**, 347–377 (2007).
[12] A. K. Uguz, O. Ozen, and N. Aubry, "Electric field effect on a two-fluid interface instability in channel flow for fast electric times," Phys. Fluids **20**, 031702 (2008).
[13] A. K. Uguz and N. Aubry, "Quantifying the linear stability of a flowing electrified two-fluid layer in a channel for fast electric times for normal and parallel electric fields," Phys. Fluids **20**, 092103 (2008).
[14] U. Seifert, "The concept of effective tension for fluctuating vesicles," Z. Phys. B: Condens. Matter **97**, 299–309 (1995).
[15] Y.-N. Young, S. Veerapaneni, and M. J. Miksis, "Long-wave dynamics of an inextensible planar membrane in an electric field," J. Fluid Mech. **751**, 406–431 (2014).
[16] J. T. Schwalbe, P. M. Vlahovska, and M. Miksis, "Lipid membrane instability driven by capacitive charging," Phys. Fluids **23**, 04170 (2011).
[17] J. Seiwert, M. J. Miksis, and P. M. Vlahovska, "Stability of biomimetic membranes in dc electric fields," J. Fluid Mech. **706**, 58–70 (2012).
[18] F. Ziebert and D. Lacoste, "A planar lipid bilayer in an electric field: Membrane instability, flow field, and electrical impedance," Adv. Planar Lipid Bilayers Liposomes **14**, 63–95 (2011).
[19] J. Seiwert and P. M. Vlahovska, "Instability of a fluctuating membrane driven by an ac electric field," Phys. Rev. E **87**, 022713 (2013).
[20] A. E. Hosoi and L. Mahadevan, "Peeling, healing, and bursting in a lubricated elastic sheet," Phys. Rev. Lett. **93**, 137802 (2004).
[21] C. S. Yih, "Instability due to viscous stratification," J. Fluid Mech. **27**, 337 (1967).
[22] S. A. Roberts and S. Kumar, "AC electrohydrodynamic instabilities in thin liquid films," J. Fluid Mech. **631**, 255–279 (2009).
[23] S. A. Roberts and S. Kumar, "Electrohydrodynamic instabilities in thin liquid trilayer films," Phys. Fluids **22**, 122012 (2010).
[24] A.-F. Bitbol, N. Puff, Y. Sakuma, M. Imai, J.-B. Fournier, and M. I. Angelova, "Lipid membrane deformation in response to a local pH modification: Theory and experiments," Soft Matter **8**, 6073–6082 (2012).